Electronic Supplementary Material (ESI) for Journal of Materials Chemistry C.

Efficient Orange Organic Light-Emitting Diodes Employing a Central Aniline Bridged Multiresonant Thermally Activated Delayed Fluorescence Emitter

Sen Wu,[a] *Ya-Nan Hu,*[b] *Jingxiang Wang*[a], *Dianming Sun,*[a*] *Kai Wang,*[b] *Xiao-Hong Zhang*[b,c*] and *Eli Zysman-Colman*[a*]

[a]Organic Semiconductor Centre, EaStCHEM School of Chemistry, University of St Andrews, St Andrews, Fife, UK, KY16 9ST, Fax: +44-1334 463808; Tel: +44-1334 463826; E-mail: eli.zysman-colman@st-andrews.ac.uk; sd235@st-andrews.ac.uk.

[b]Institute of Functional Nano & Soft Materials (FUNSOM), Joint International Research Laboratory of Carbon-Based Functional Materials and Devices, Soochow University, Suzhou, Jiangsu 215123, P. R. China. E-mail: xiaohong_zhang@suda.edu.cn.

[c]Jiangsu Key Laboratory of Advanced Negative Carbon Technologies, Soochow University, Suzhou, 215123, Jiangsu, P. R. China.

Table of Contents

General methods

General Synthetic Procedures. Br-DiKTa was synthesized according to the literature reported method.[1] The other reagents and solvents were obtained from commercial sources and used as received unless otherwise stated. Air-sensitive reactions were run under a nitrogen atmosphere using Schlenk techniques. Dry solvents used in the reaction were obtained from a MBRAUN SPS5 solvent purification system. Flash column chromatography was carried out using silica gel (Silia-P from Silicycle, 60 Å, 40-63 μm). Analytical thin-layer-chromatography (TLC) was performed with silica plates with aluminium backings (250 μm with F-254 indicator). TLC visualization was accomplished by 254/365 nm UV lamp. HPLC was conducted on a Shimadzu LC-40 HPLC system. HPLC traces were performed using a Shim-pack GIST 3μm C18 reverse phase analytical column. ^{1}H and ^{13}C and NMR spectra were recorded on a Bruker Advance spectrometer (500 MHz for ^{1}H and 126 MHz for ^{13}C). The following abbreviations have been used for multiplicity assignments: "s" for singlet, "d" for doublet, "t" for triplet, "m" for multiplet, "dd" for doublet of doublets, "dt" for doublet of triplets. ^{1}H and ^{13}C NMR spectra were referenced to the solvent peaks). Melting points were measured using open-ended capillaries on an Electrothermal 1101D Mel-Temp apparatus and are uncorrected. MALDI coupled time-of-flight mass spectrometry (HRMS) was performed at Soochow University. Elemental analyses were performed by Dr. Joe Casillo at the University of Edinburgh.

Quantum chemical calculations. The calculations were performed using Density Functional Theory (DFT) within Gaussian 16[2] as well as the second order algebraic diagrammatic construction Spin-Component Scaling (ADC(2)-SCS)[3] method using the Turbomole/7.5 package.[4] For the DFT calculations, the ground-state and excited singlet state were optimized using the PBE0[5] functional and the 6-31G(d,p) basis set,[6] and the excited-state calculations were performed using Time-Dependent DFT within the Tamm-Dancoff approximation (TDA-DFT)[7,8] with the same functional and basis set as for the ground-state geometry optimization in the gas phase. Spin-orbit coupling matrix elements SOCME were calculated based on the optimized excited triplet state geometry. Spin-orbit coupling matrix elements between singlet and triplet excited states were calculated using the PySOC program. The molecular orbital distributions were visualized with Gaussview 5.0.[9] For the ADC(2) calculations, the ground states was optimized using the ADC(2)-SCS functional and the cc-pVDZ basis set in the gas phase based on the geometry calculated by DFT.[10] Vertical transitions to the excited states were performed based on the ground-state optimized structure. Difference density plots were used to visualize change in electronic density between the ground and excited state and were visualized using the VESTA package.[11] The RMSD of ground state and excited singlet state was visualized using VMD program.[12] All calculations were submitted using the Silico v4 software package.[13–16]

Electrochemistry measurements. Cyclic Voltammetry (CV) analysis was performed on an Electrochemical Analyzer potentiostat model 620E from CH Instruments at a sweep rate of 100 mV/s. Differential pulse voltammetry (DPV) was conducted with an increment potential of 0.004 V and a pulse amplitude, width, and period of 50 mV, 0.05, and 0.5 s, respectively. Samples were prepared in DCM solutions, which were degassed by sparging with DCM-saturated nitrogen gas for 5 minutes prior to measurements. All measurements were performed using 0.1 M DCM solution of tetra-*n*-butylammonium hexafluorophosphate, [^{n}Bu$_4$N]PF$_6$. An Ag/Ag$^+$ electrode was used as the reference electrode while a platinum electrode and a platinum wire were used as the working electrode and counter electrode, respectively. The redox potentials are reported relative to a saturated calomel electrode (SCE) with a ferrocenium/ferrocene (Fc/Fc$^+$) redox couple as the internal standard (0.46 V vs SCE).[17] The HOMO and LUMO energies were determined using the relation $E_{HOMO/LUMO} = -(E_{ox} / E_{red} + 4.8)$ eV, where E_{ox} and E_{red} are the onset of anodic and cathodic peak potentials, respectively calculated from DPV relative to Fc/Fc$^+$.[18]

Photophysical measurements. Optically dilute solutions of concentrations on the order of 10^{-5} or 10^{-6} M were prepared in spectroscopic grade solvents for absorption and emission analysis. Absorption spectra were recorded at room temperature on a Shimadzu UV-2600 double beam spectrophotometer with a 1 cm quartz cuvette. Molar absorptivity determination was verified by linear regression analysis of values obtained from at least four independent solutions at varying concentrations range from 3.0×10^{-6} to 1.0×10^{-5} with absorbance ranging from 0.025 to 0.100. For emission studies, steady-state emission and time-resolved emission spectra were recorded at room temperature using an Edinburgh Instruments FS5 fluorimeter. Samples were excited at 340 nm for steady-state measurements and 379 for time-resolved PL decays. Photoluminescence quantum yields for solutions were determined using the optically dilute method, in which four sample solutions with absorbances of ca. 0.10, 0.075, 0.050 and 0.025 at 360 nm were used.[19] The Beer-Lambert law was found to remain linear at the concentrations of the solutions. For each sample, linearity between absorption and emission intensity was verified through linear regression analysis with the Pearson regression factor (R^2) for the linear fit of the data set surpassing 0.9. Individual relative quantum yield values were calculated for each solution and the values reported represent the slope obtained from the linear fit of these results. The quantum yield of the sample, Φ_{PL}, was determined using the equation $\Phi_{PL} = (\Phi_r * \frac{A_r}{A_s} * \frac{I_s}{I_r} * \frac{n_s^2}{n_r^2})$,[19] where A stands for the absorbance at the excitation wavelength (λ_{exc} = 340 nm), I is the integrated area under the corrected emission curve and n is the refractive index of the solvent with the subscripts "s" and "r" representing sample and reference respectively. Φ_r is the absolute quantum yield of the external reference quinine sulfate (Φ_r = 54.6% in 1 *N* H_2SO_4).[20] An integrating sphere (Edinburgh Instruments FS5, SC30 module) was employed for the

photoluminescence quantum yield measurements of thin film samples. The Φ_{PL} of the films were then measured in air and in N_2 by purging the integrating sphere with N_2 gas flow for 2 min. The photophysical properties of the film samples were measured using an Edinburgh Instruments FS5 fluorimeter. Time-resolved PL measurements of the thin films were carried out using the multi-channel scaling (MCS) and time-correlated single-photon counting (TCSPC) technique. The samples were excited at 379 nm by a pulsed laser and were kept in a vacuum of $< 8 \times 10^{-4}$ mbar. The singlet and triplet state energies in 2-MeTHF glass and in doped film were determined from the onset values of the steady-state photoluminescence PL (SSPL) and phosphorescence spectra at 77 K. The singlet-triplet energy gap (ΔE_{ST}) was estimated from the difference in energy of the steady-state PL and phosphorescence spectra. The samples were excited by a xenon flashlamp emitting at 340 nm (EI FS5, SC-70). Phosphorescence spectra were measured with a time-gated window of 1-10 ms.

Fitting of time-resolved luminescence measurements: Time-resolved PL measurements were fitted to a sum of exponentials decay model, with chi-squared (χ^2) values between 1 and 2, using the EI FS5 Each component of the decay is assigned with a weight, (w_i), which is the contribution of the emission from each component to the total emission.

The average lifetime was then calculated using the following expressions:

1. Two exponential decay model:

$$\tau_{AVG} = \tau_1 w_1 + \tau_2 w_2 \quad \text{(S1)}$$

with weights defined as $w_1 = \frac{A1\tau_1}{A1\tau_1 + A2\tau_2}$ and $w_2 = \frac{A2\tau_2}{A1\tau_1 + A2\tau_2}$ where A_1 and A_2 are the preexponential-factors of each component.

2. Three exponential decay model:

$$\tau_{AVG} = \tau_1 w_1 + \tau_2 w_2 + \tau_3 w_3 \quad \text{(S2)}$$

with weights defined as $w_1 = \frac{A1\tau_1}{A1\tau_1 + A2\tau_2 + A3\tau_3}$, $w_2 = \frac{A2\tau_2}{A1\tau_1 + A2\tau_2 + A3\tau_3}$ and $w_3 = \frac{A3\tau_3}{A1\tau_1 + A2\tau_2 + A3\tau_3}$ where A_1, A_2 and A_3 are the preexponential-factors of each component.

OLED Fabrication and Characterization: The OLED devices were fabricated in a bottom-emitting structure via thermal evaporation in a high vacuum at a base pressure of $<5\times10^{-7}$ mbar. A pre-patterned glass substrate coated with indium doped tin oxide (ITO) was cleaned sequentially by ultrasonication in acetone, and isopropanol for 15 minutes. The temperature of ultrasonication bath was set at 60-70 °C. The cleaned substrate was exposed to oxygen plasma for 3 min to remove all dust and organics on the ITO surface and to increase the work function of ITO anode for better hole injection from the anode to organic layer. The substrate was loaded in the thermal evaporator. Organic layers were deposited at a rate of 0.3-1.0 Å/s, monitored using a quartz crystal. The electron injection layer, LiF, was deposited at a rate of 0.05 Å/s, while the Al cathode was deposited initially with a rate of 0.5 Å/s to obtain 10 nm thickness

and after that the rate of Al cathode was increased to 3 Å/s. Two custom-made shadow masks were used to define the area of the evaporations. The organic layers and LiF were evaporated with a same shadow mask, but Al were evaporated with the other mask. The active area of the OLED was 2 mm^2, determined by the spatial overlap of the anode and cathode electrodes. All the devices were encapsulated with glass lids and UV epoxy resin inside a N_2 filled globe box. The luminance-current-voltage characteristics were measured in an ambient environment using a Keithley 2400 source meter and a homemade photodiode circuit connected to a Keithley 2000 multimeter for the voltage reading. The external quantum efficiency was calculated assuming Lambertian emission pattern for the OLEDs. The electroluminescence spectra were recorded by an Andor DV420-BV CCD spectrometer.

Literature study

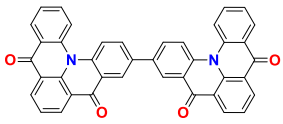

DDiKTa

Mater. Chem. Front., **2020**, *4*, 2018--2022

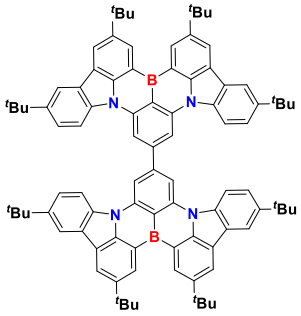

***p*-CzB**

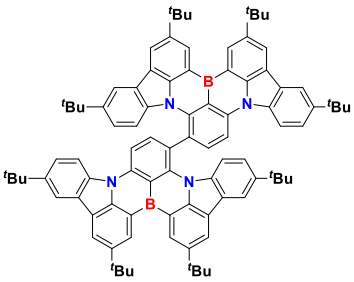

***m*-CzB**

J. Mater. Chem. C, **2023**, *11*, 917–922

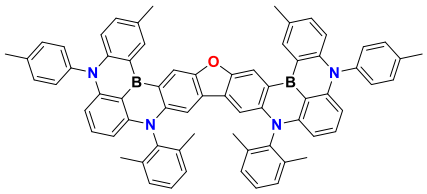

DBF-DBN

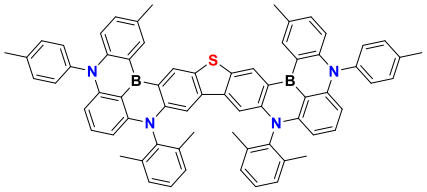

DBT-DBN

Chem. Commun., **2023**, *59*, 5126–5129

Figure **S1**. Molecular structures of dimeric MR-TADF emitters discussed in the main text.

Experimental Section

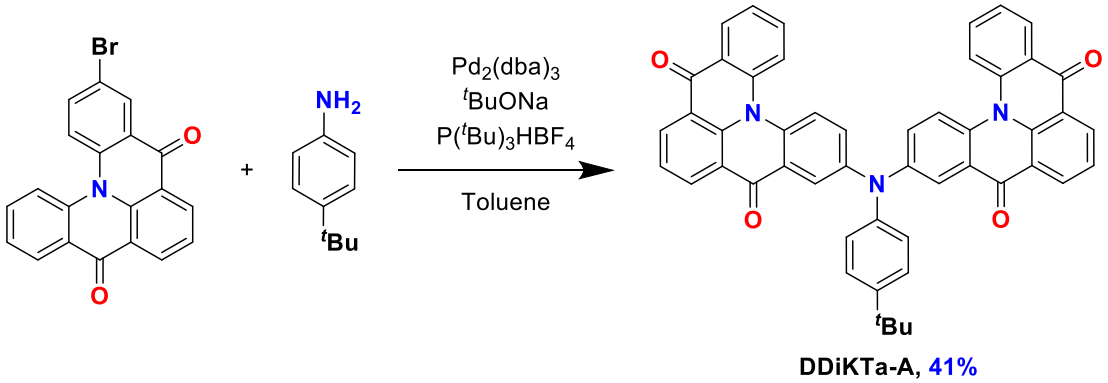

DDiKTa-A, 41%

Scheme **S2**. The synthesis route of **DiKTa-A**.

3,3'-((4-(*tert*-butyl)phenyl)azanediyl)bis(quinolino[3,2,1-de]acridine-5,9-dione) (**DDiKTa-A**) 4-(*tert*-butyl)aniline (150 mg, 1.0 mmol, 1 equiv.), **DiKTa** (945.3 mg, 2.5 mmol, 2.5 equiv.), sodium *tert*-butoxide (289.8, 3.0 mmol, 3.0 equiv.), $Pd_2(dba)_3$ (46.0 mg, 0.05 mmol, 0.05 equiv.) and [^{t}Bu$_3$PH]BF_4 (29.1 mg, 0.1 mmol, 0.1 equiv.) were added to a Schlenk flask containing 10 mL of anhydrous toluene. After degassing the flask, the reaction system was placed under a nitrogen atmosphere. The mixture was heated at 115 °C for 24 h. After cooling to room temperature, DCM (200 mL) was added to the mixture. The mixture was washed with a saturated NaCl aqueous solution (2× 200 mL). The collected organic phase was dried over anhydrous sodium sulfate and concentrated under reduced pressure. The collected crude product was purified by silica gel column chromatography (EtOAc: DCM = 1:20, $\mathbf{R_f}$: 0.30) to afford the target compounds with red powder. **Yield**. 0.32 mg, 43%. **R_f:** 0.4 (DCM). **Mp**: 259-261°C. **^{1}H NMR (500 MHz, $CDCl_3$)** δ 8.77 (dd, J = 7.6, 1.5 Hz, 2H), 8.72 (dd, J = 7.6, 1.5 Hz, 2H), 8.52 (dd, J = 7.9, 1.2 Hz, 2H), 8.23 – 8.18 (m, 4H), 8.09 (d, J = 9.2 Hz, 2H), 7.75 – 7.70 (m, 2H), 7.65 (t, J = 7.7 Hz, 2H), 7.51 (dt, J = 11.3, 5.5 Hz, 4H), 7.40 (d, J = 8.6 Hz, 2H), 7.16 (d, J = 8.6 Hz, 2H), 1.38 (s, 9H). **^{13}C NMR (126 MHz, $CDCl_3$)** δ 178.55, 178.20, 148.03, 144.74, 143.37, 139.74, 139.02, 135.02, 133.10, 133.06, 132.77, 128.17, 127.88, 127.65, 127.01, 126.33, 125.13, 124.99, 123.52, 123.39, 123.14, 121.87, 120.38, 12f0.19, 34.55, 31.43. **MALDI-TOF MS [M^+]**: Calculated: 739.830 ($C_{50}H_{33}N_3O_4^+$); Found: 739.611. **Anal. Calcd. For $C_{50}H_{33}N_3O_4$**: C 81.17%, H 4.50%, N 5.68% **Found**: C 81.44%, H 4.62%, N 5.63%. 99.90% pure on HPLC analysis, retention time 16.318 minutes in 75% MeCN and 20% H_2O system.

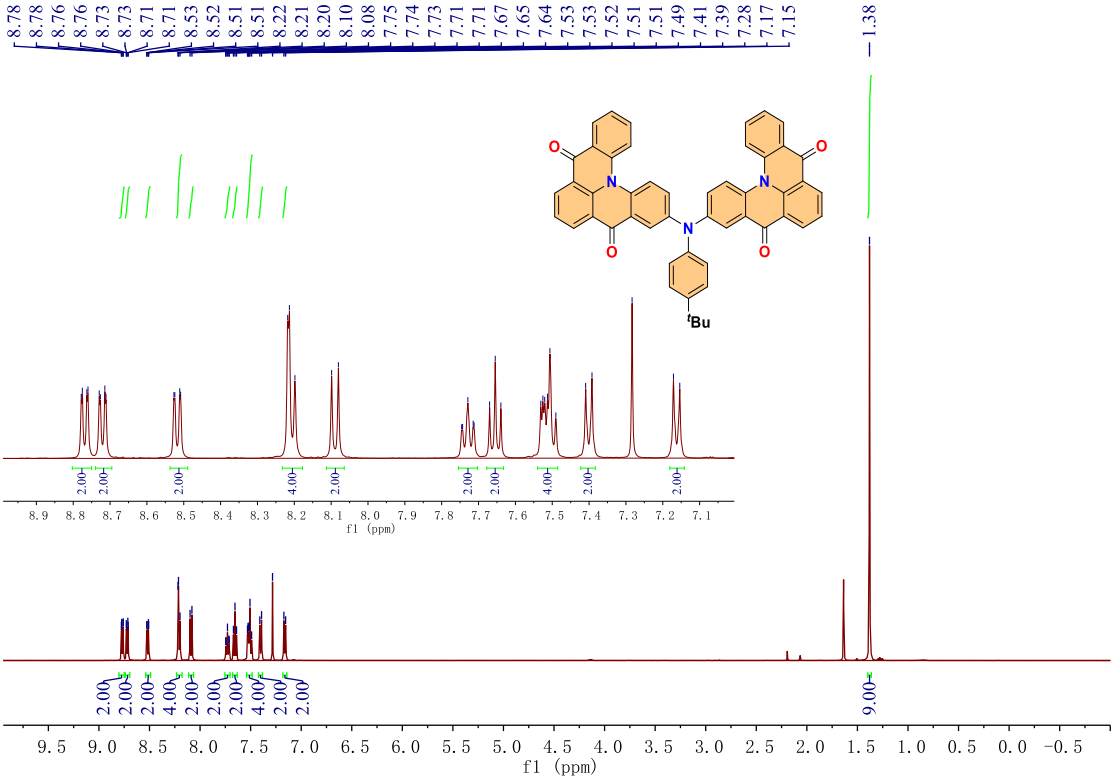

Figure **S1**. ^{1}H-NMR of **DDiKTa-A** in $CDCl_3$.

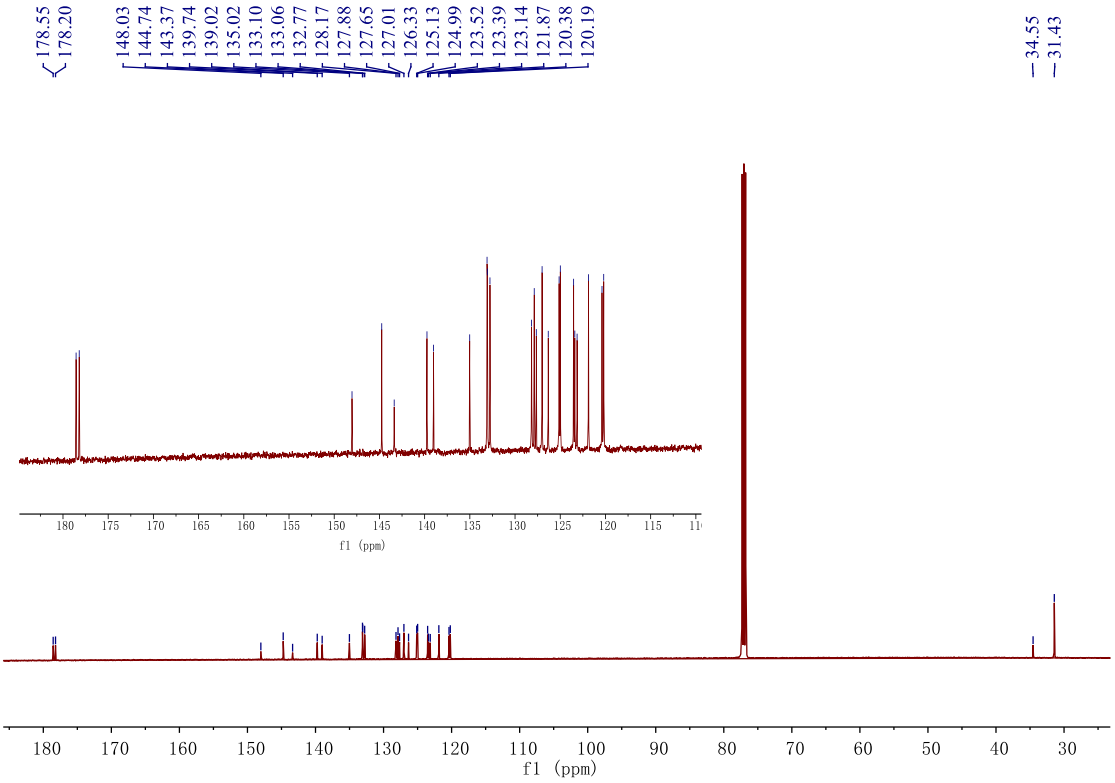

Figure **S2**. ^{13}C-NMR of **DDiKTa-A** in $CDCl_3$.

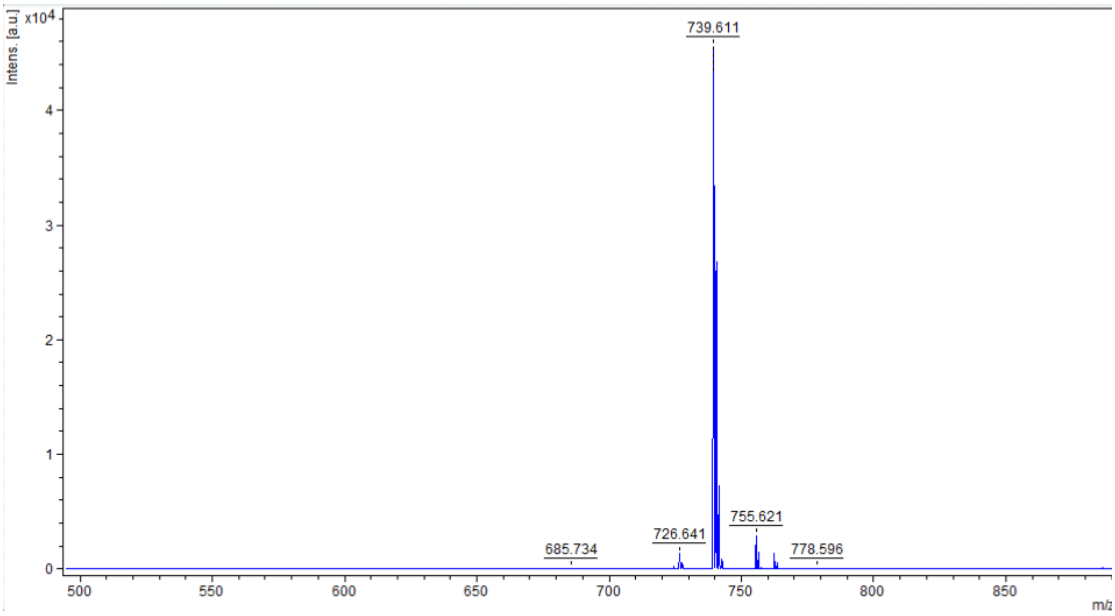

Figure **S3**. MALDI TOF MS spectrum of **DDiKTa-A**.

Name of Compound	DDiKTa-A
Molecular formula	C50H33N3O4
Stability	
Hazards	
Other Remarks	

Analysis type:

Single ☐ **Duplicate** ☑ **Triplicate** ☐

Analysis Result:

Element	Expected %	Found (1)	Found (2)	Found (3)
Carbon	81.17	80.53	82.34	
Hydrogen	4.50	4.59	4.65	
Nitrogen	5.68	5.59	5.66	
Oxygen				

Figure **S4**. Elemental analysis of **DDiKTa-A**. The average values are: C 81.44%, H 4.62%, N 5.63%.

Sample Name	: ddikta-nph		
Sample ID	:		
Method Filename	: 75% Acetonitrile 25 Water 20 mins.lcm		
Batch Filename	: 90-10.lcb		
Vial #	: 1-9	Sample Type	: Unknown
Injection Volume	: 1 uL		
Date Acquired	: 24/03/2022 23:56:37	Acquired by	: System Administrator
Date Processed	: 25/03/2022 00:16:39	Processed by	: System Administrator

<Chromatogram>

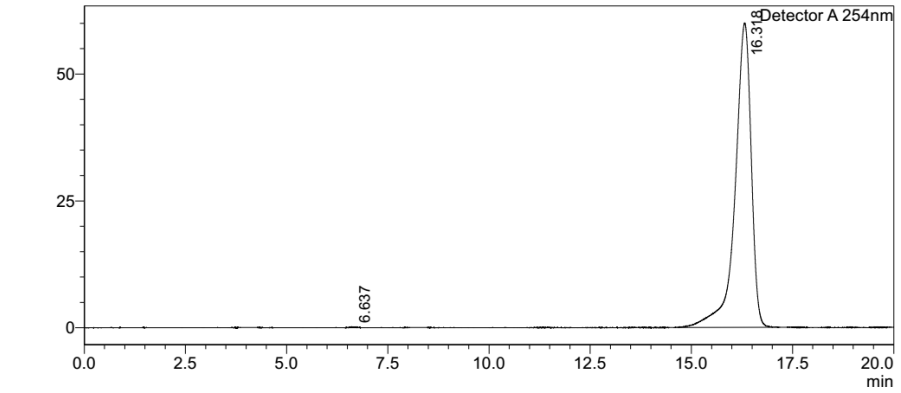

<Peak Table>

Detector A 254nm

Peak#	Ret. Time	Area	Height	Area%	Area/Height	Width at 5% Height
1	6.637	1703	168	0.102	10.147	0.293
2	16.318	1662275	59947	99.898	27.729	1.100
Total		1663978	60115	100.000		

Figure **S5**. The HPLC spectrum of **DDiKTa-A**

Computations

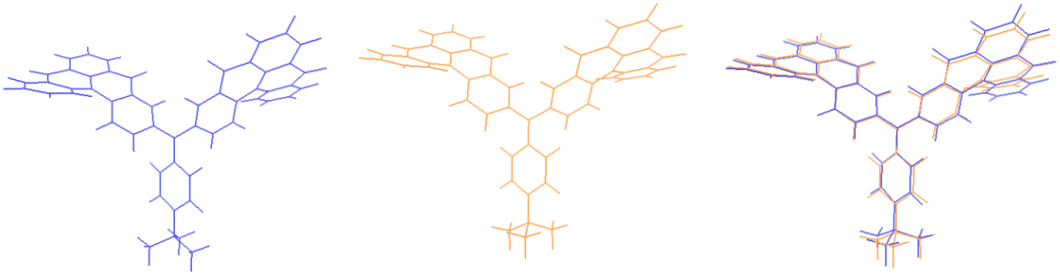

Figure **S6**. Optimized structures of the ground state (S_0) and excited singlet state (S_1) and the geometric difference between the S_0 and S_1 states. The root mean square deviation (RMSD) value between the two configurations is 0.2757.

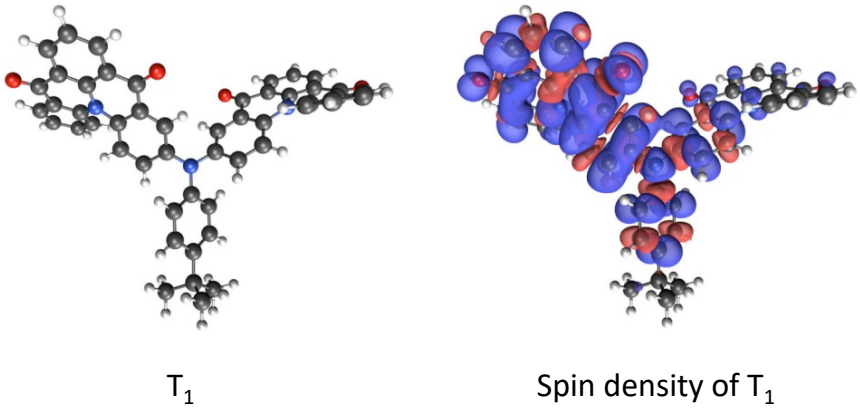

Figure **S7**. T_1 optimized geometry and triplet spin density of **DDiKTa-A** calculated in the gas phase at the at the uPBE0/6-31G(d,p) level (isovalue: 0.0004).

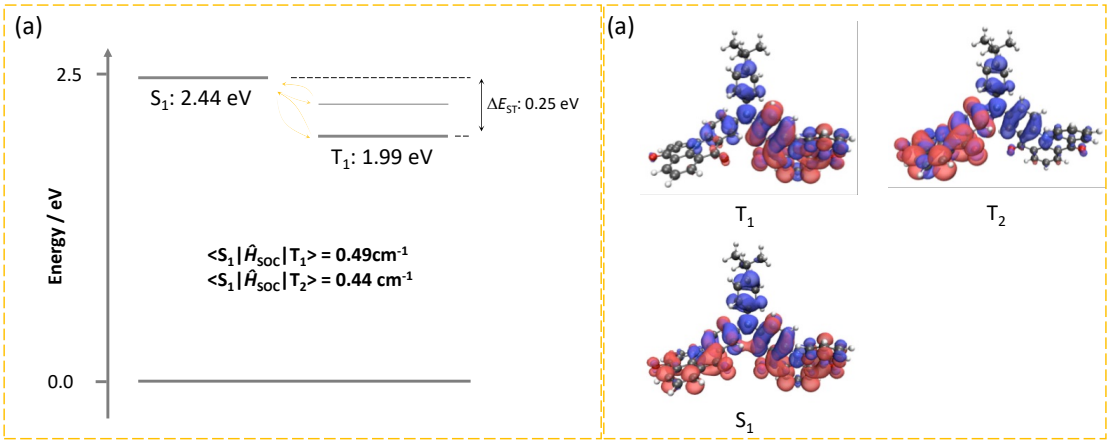

Figure **S8**. (a) Spin-orbit coupling matrix element (SOCME) and (b) the natural transition orbitals (NTOs) for **DDiKTa-A** based on optimized triplet state geometry.

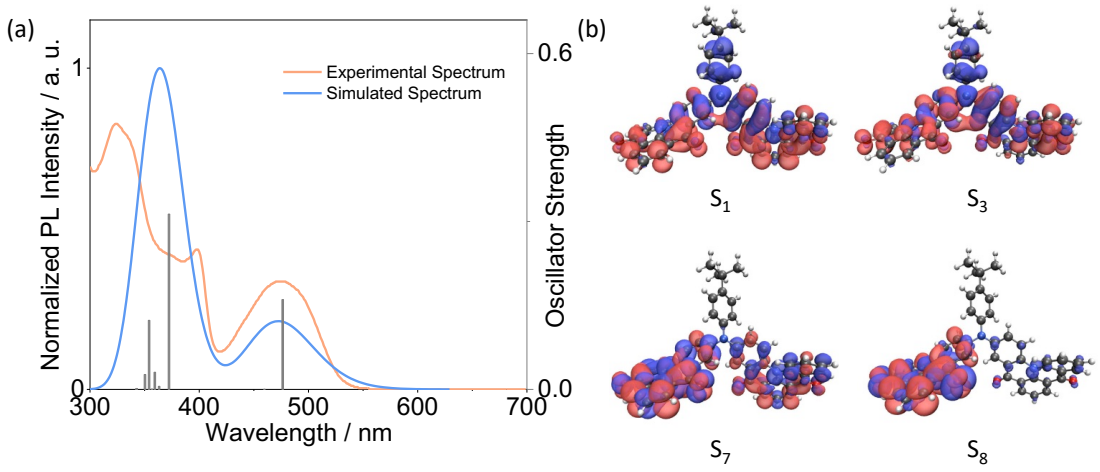

Figure **S9**. (a) Experimental absorption spectra for **DDiKTa-A** and simulated spectra and related oscillator strength of the first 10 singlet excited states. (b) the natural transition orbitals (NTOs) for **DDiKTa-A** based on the optimized ground-state geometry.

Photophysical characterization

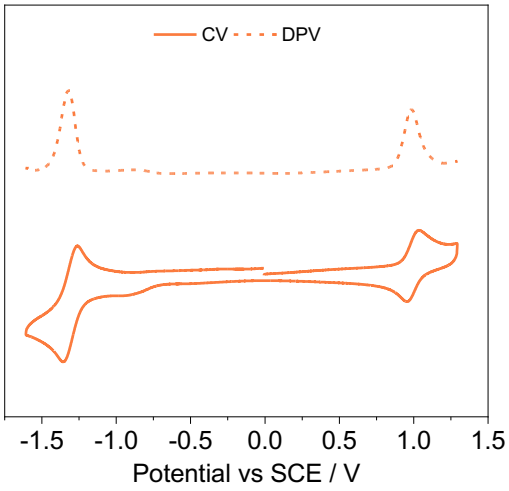

Figure **S10**. Cyclic voltammogram (CV) and differential pulse voltammetry (DPV) in degassed DCM with 0.1 M [^{n}Bu$_4$N]PF$_6$ as the supporting electrolyte and Fc/Fc$^+$ as the internal reference versus SCE (0.46 V vs. SCE). [18]

Table **S1.** Electrochemical data

Material	E_{ox} /V[a]	E_{red} /V[a]	ΔE /V[b]	HOMO / eV[c]	LUMO /eV[c]
DDiKTa-A	0.98	-1.32	2.30	-5.32	-3.02
DiKTa	1.78	-1.35	3.03	-6.12	-2.99

[a] E_{ox} and E_{red} are the peak of anodic and cathodic potentials from DPV versus SCE. In degassed DCM with 0.1 M [^{n}Bu$_4$N]PF$_6$ as the supporting electrolyte and Fc/Fc$^+$ as the internal reference (0.46 V vs. SCE).[17] [b] $\Delta E_g = E_{ox}$-E_{red}. [c] $E_{HOMO/LUMO}$ = -(E_{ox} / E_{red} vs. Fc/Fc$^+$ + 4.8) eV.[18]

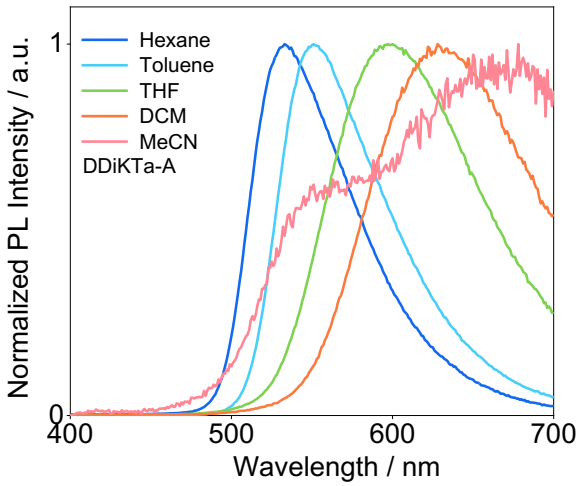

Figure **S11**. Solvatochromic PL of **DDiKTa-A**, λ_{exc} = 340 nm.

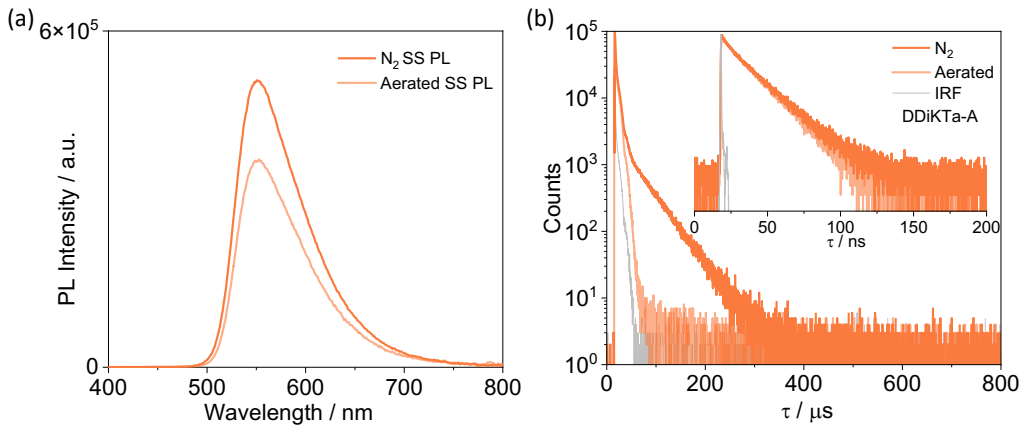

Figure **S12**. Aerated and degassed Comparison of (a) steady-state PL for **DDiKTa-A** (λ_{exc} = 340 nm) and (b) Time-resolved PL decays (inset is the PL decay of prompt component measured by TCSPC method) in toluene solution, λ_{exc}= 375 nm.

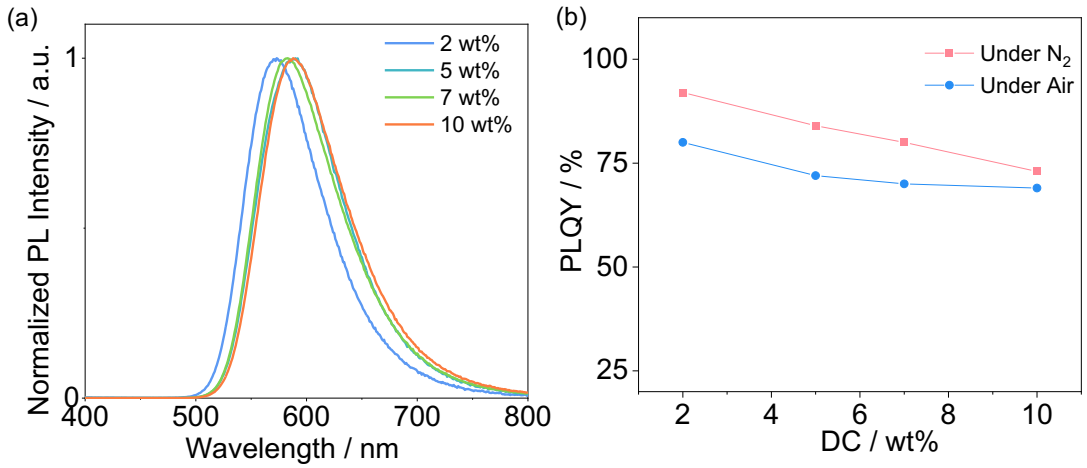

Figure **S13**. (a) Concentration-dependent PL of **DDiKTa-A** in mCP doped films; (b) Concentration-dependent Φ_{PL} of **DDiKTa-A** in mCP doped films under air and nitrogen, λ_{exc} = 340 nm. DC = doping concentration.

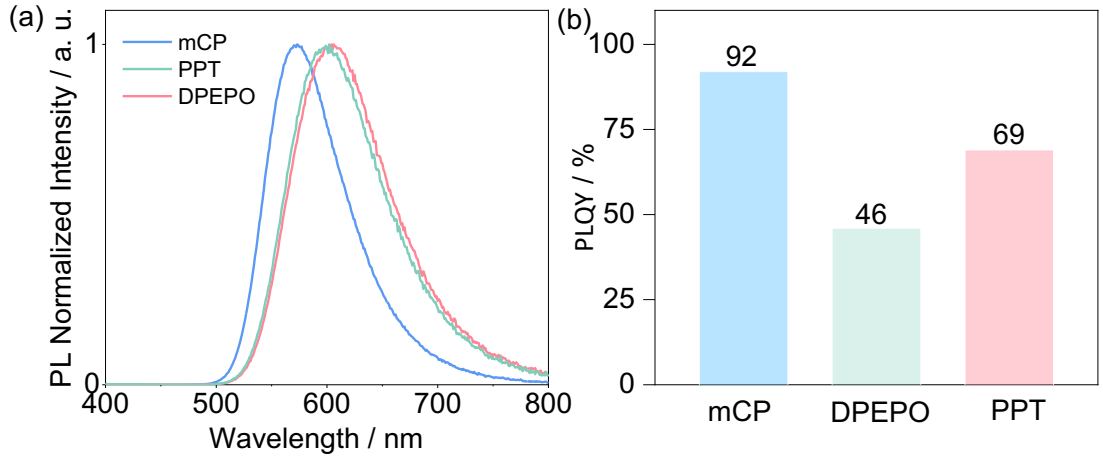

Figure **S14**. (a) SS PL in different host systems of **DDiKTa-A**; (b) Φ_{PL} of **DDiKTa-A** in different host systems under nitrogen, λ_{exc}= 340 nm.

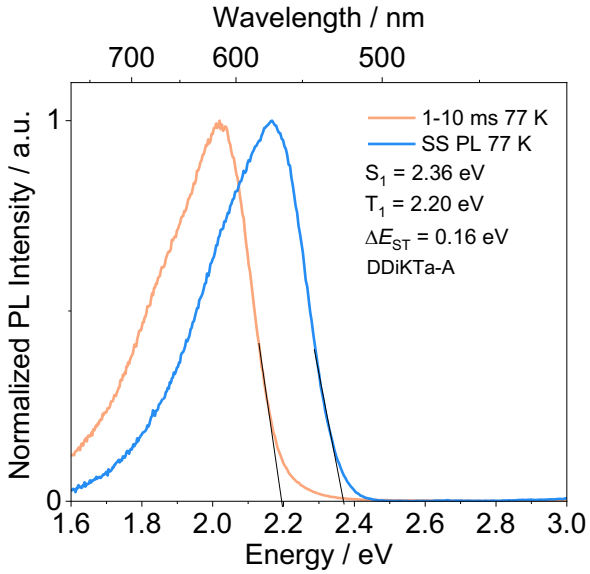

Figure **S15**. Steady-state PL and phosphorescence spectra (1-10 ms) of **DDiKTa-A** in 2 wt% doped films in mCP at 77 K, λ_{exc}= 340 nm.

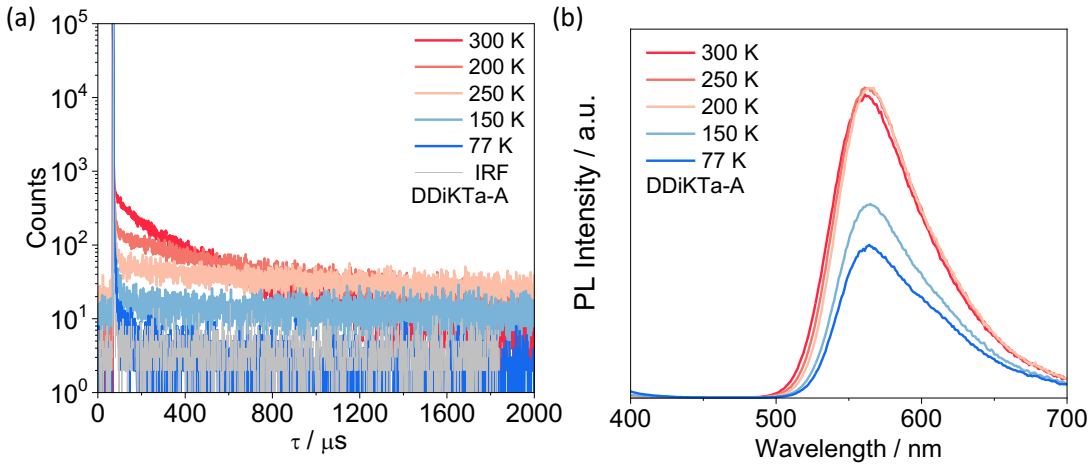

Figure **S16**. Temperature-dependent (a) Time-resolved PL decay, λ_{exc} = 375 nm; and (b) Steady-state PL of **DDiKTa-A**, λ_{exc} = 340 nm.

For a TADF system, the main exciton loss channels are either singlet or triplet nonradiative transition processes. Considering the Φ_{PL} of 92% for **DDiKTa-A**, the singlet nonradiative transition process (k_{nr}^{S}) can was neglected and assumed to be 0; therefore, the exciton loss can be attributed to only the triplet nonradiative transition processes (k_{nr}^{T}). The kinetics parameters were calculated according to the following equations and summarized in Table **S2**.[21,22]

$$\Phi_{PL} = \Phi_p + \Phi_d \quad (1)$$

$$k_P = \frac{1}{\tau_p} \quad (2)$$

$$k_d = \frac{1}{\tau_d} \quad (3)$$

$$k_r^S = k_p \Phi_p \quad (4)$$

$$k_{ISC} = k_p(1 - \Phi_p) \quad (5)$$

$$k_{RISC} = \frac{k_p k_d}{k_{ISC}} \frac{\Phi_d}{\Phi_p} \quad (6)$$

$$k_{nr}^T = k_d - \Phi_p k_{RISC} \quad (7)$$

Where the Φ_p and Φ_d are the prompt fluorescence and delayed fluorescence quantum efficiencies; k_p is the rate constant of prompt fluorescence; k_d is the rate constant of delayed fluorescence; k_r^S is the radiative decay rate constant of S_1; k_{nr}^T is the non-radiative decay rate constant of T_1; k_{ISC} is the intersystem crossing rate constant; k_{RISC} is the reverse intersystem crossing rate constant.

Table **S2.** Summary of kinetics parameters.

Compounds	Φ_P /%	Φ_d /%	k_p / 10^7 s^{-1}	k_d / 10^3 s^{-1}	k_r^S /10^7 s^{-1}	k_{nr}^T /10^3 s^{-1}	k_{ISC} /10^7 s^{-1}	k_{RISC} /10^4 s^{-1}
DDiKTa-A[a]	30	14	6.13	24.4	1.84	195	4.29	1.63
DDiKTa-A[b]	17	75	6.62	3.58	1.13	0.35	5.50	1.91
DDiKTa-A[c]	12	86	3.13	6.71	3.75	0.15	2.75	5.47
DiKTa[23]	7	39	2.08	0.41	1.44	2.40	1.94	2.52

[a] Measured in toluene solution (1×10^{-5} M); [b] Measured in spin-coated 2 wt% doped thin films in mCP; [c] Measured in spin-coated 5 wt% doped thin films in 4CzIPN/mCP (10:85).

Devices

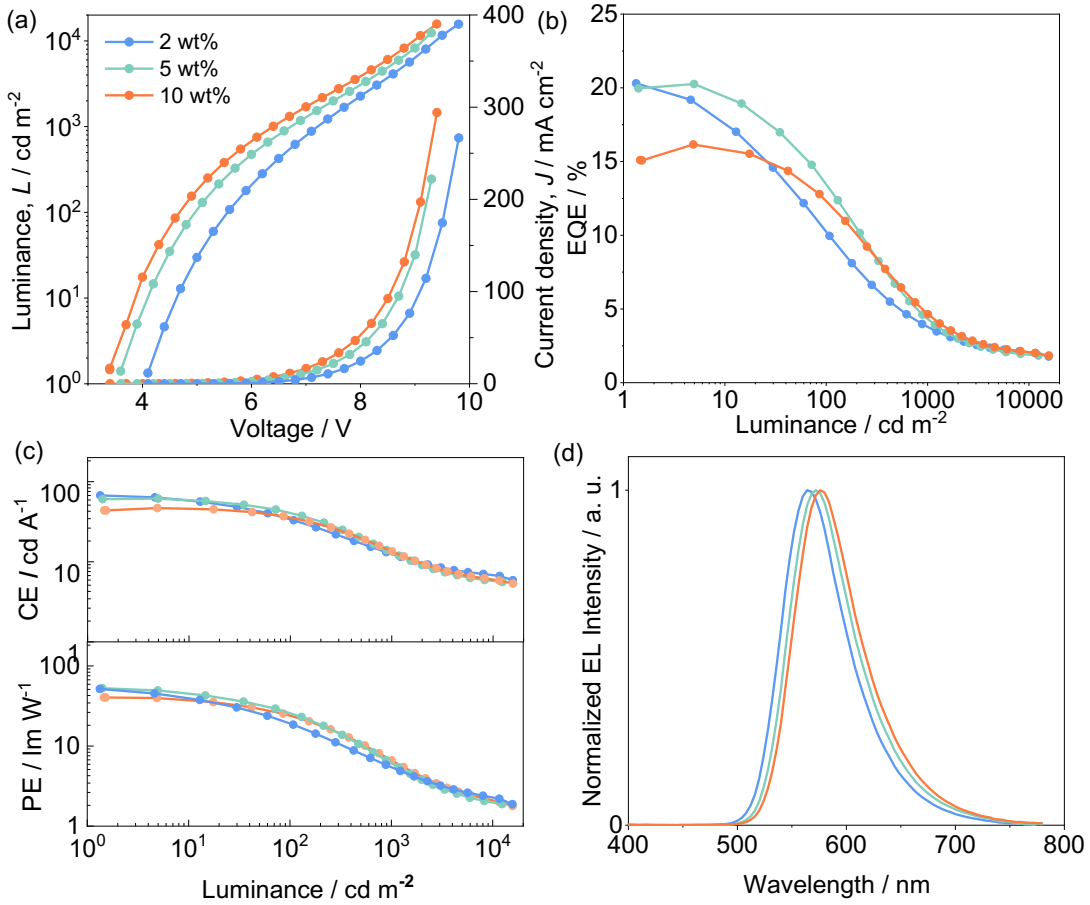

Figure **S17**. (a) Current density and luminance versus voltage characteristics for the devices. (b) External quantum efficiency versus luminance curves for the devices. (c) Current and power efficiency versus luminance curves for the devices. (d) Electroluminescence spectra of the devices. Device structure: ITO/ TAPC (35 nm)/TCTA (10 nm)/CzSi (10 nm)/x wt% **DDiKTa-A**: mCP (20 nm) /TmPyPB (40 nm)/LiF (1 nm)/Al (100 nm)

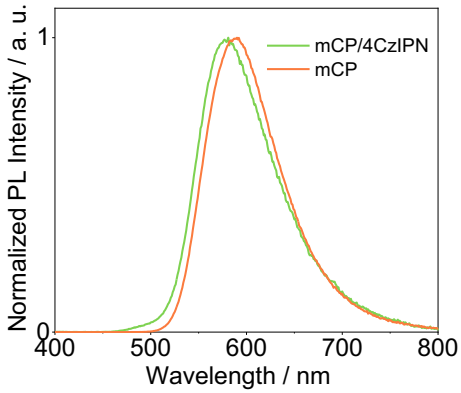

Figure **S18**. Steady-state PL comparation between 5 wt% **DDiKTa-A** in mCP film and 4CzIPN/mCP film. λ_{exc} = 340 nm.

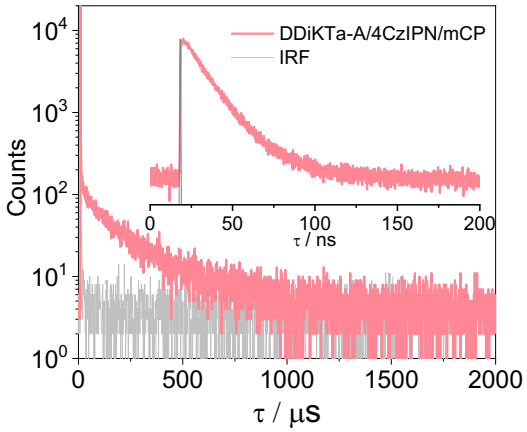

Figure **S19**. Time-resolved PL decays (inset is the PL decay of prompt component measured by TCSPC method) measured by MCS method under vacuum of 5 wt% **DDiKTa-A** and 10 wt% **4CzIPN** doped films in mCP, λ_{exc}= 375 nm.

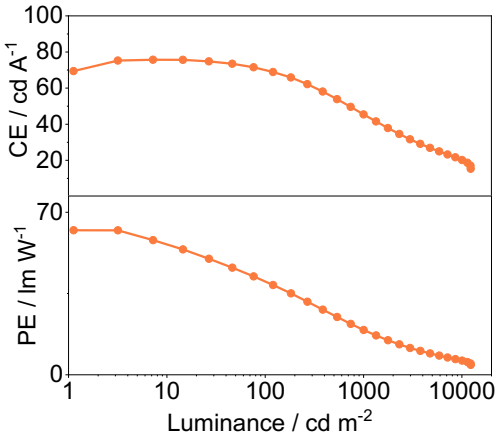

Figure **S20**. Current and power efficiency versus luminance curves for the device. Emissive layer: **DDiKTa-A**/4CzIPN/mCP = 5:10:85.

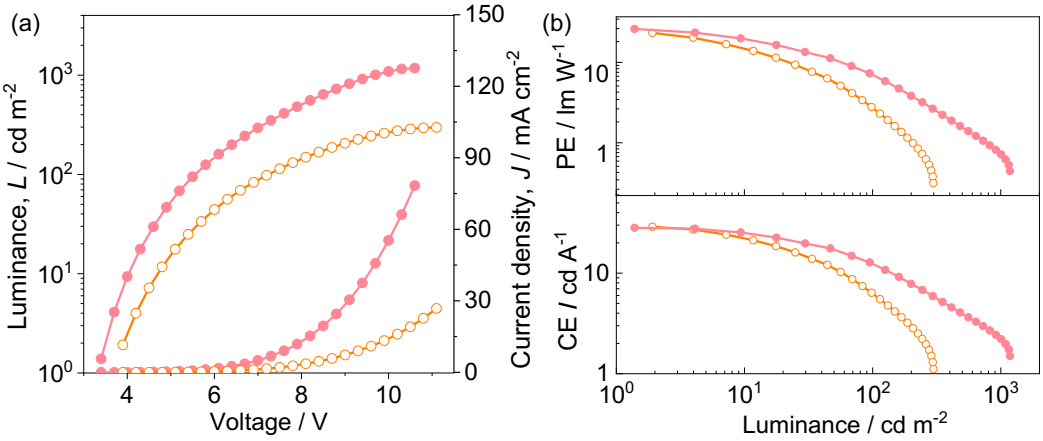

Figure **S21**. (a) Current density and luminance versus voltage characteristics for the devices. (c) Current and power efficiency versus luminance curves for the devices. Emissive layer: 5 wt% and 10 wt% **DDiKTa-A**/DPEPO.

Table **S3**. Key parameters of reported devices based on carbonyl-based MR-TADF OLEDs (λ_{EL} >500 nm).

Emitters[a]	**λ_{EL} / nm**	**EQE_{max} / %**	**EQE_{100} / %**	**Roll-off / % at EQE_{100}**	**L_{max} / cd m^{-2}**	**Reference**
DDiKTa-A	572	20.3	13.2	13.2	12 390	This Work
DDiKTa-A (HF)	574	24.3	22.5	22.5	12 310	
3DPA-DiKTa (HF)	613	17.9	8.7	51.3	46 003	24
3TPA-DiKTa (HF)	551	30.0	27.4	8.7	112 190	
Cz-DiKTa	511	24.9	20.4	18.1	13 260	25
3Cz-DiKTa	547	24.4	17.3	29.1	10 796	
QAD-2Cz	530	27.3	23.9	12.4	-	26
QAD-mTDPA	589	26.3	12.9	51.0	-	
DDiKTa	500	19.0	7.9	58.4	501	27
QAOCz1	516	16.9	-	-	11 320	28
QAOCz2	504	19.4	-	-	7679	
QAOCz3	500	21.1	-	-	6217	
OQAO	532	20.3	15.1	25.6		29
SQAO	564	17.8	13.6	23.6		
Sym-DiDiKTa	543	9.8	1.8	81.6	4310	30
Asym-DiDiKTa (HF)	548	19.9	9.9	50.0	53 625	
mBDPA-TOAT	600	17.3	-	-	-	31
pBDPA-TOAT	624	11.3	-	-	-	

[a] **HF** = hyperfluorescence device stack.

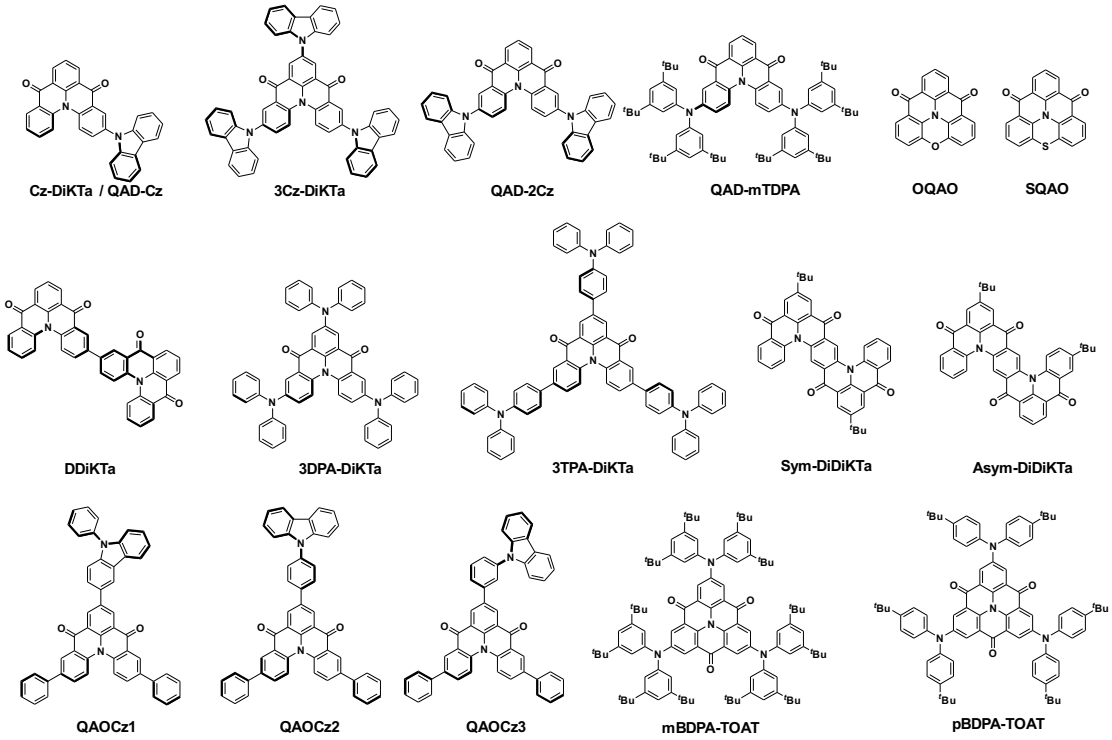

Figure **S22**. Chemical structures of carbonyl containing derivatives (the date related to these structures are summarised in Table **S3**).

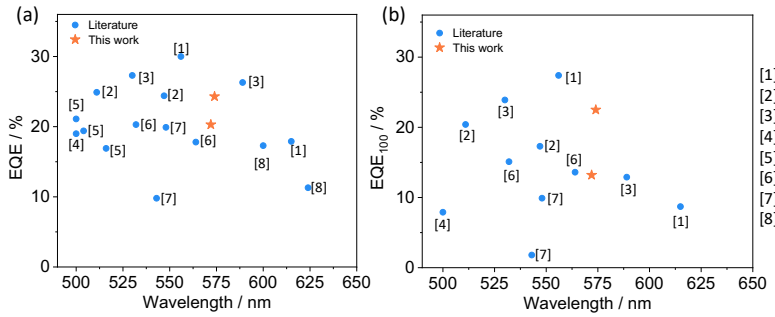

Figure **S23**. (a) EQE_{max} and (b) EQE_{100} of reported carbonyl-based MR-TADF OLEDs as a function of λ_{EL}.

Reference

1 D. Sun, S. M. Suresh, D. Hall, M. Zhang, C. Si, D. B. Cordes, A. M. Z. Slawin, Y. Olivier, X. Zhang and E. Zysman-Colman, *Mater. Chem. Front.*, 2020, **4**, 2018–2022.

2 M. J. Frisch, G. W. Trucks, H. B. Schlegel, G. E. Scuseria, M. A. Robb, J. R. Cheeseman, G. Scalmani, V. Barone, G. A. Petersson, H. Nakatsuji, X. Li, M. Caricato, A. V. Marenich, J. Bloino, B. G. Janesko, R. Gomperts, B. Mennucci, H. P. Hratchian, J. V. Ortiz, A. F. Izmaylov, J. L. Sonnenberg, Williams, F. Ding, F. Lipparini, F. Egidi, J. Goings, B. Peng, A. Petrone, T. Henderson, D. Ranasinghe, V. G. Zakrzewski, J. Gao, N. Rega, G. Zheng, W. Liang, M. Hada, M. Ehara, K. Toyota, R. Fukuda, J. Hasegawa, M. Ishida, T. Nakajima, Y. Honda, O. Kitao, H. Nakai, T. Vreven, K. Throssell, J. A. Montgomery Jr., J. E. Peralta, F. Ogliaro, M. J. Bearpark, J. J. Heyd, E. N. Brothers, K. N. Kudin, V. N. Staroverov, T. A. Keith, R. Kobayashi, J. Normand, K. Raghavachari, A. P. Rendell, J. C. Burant, S. S. Iyengar, J. Tomasi, M. Cossi, J. M. Millam, M. Klene, C. Adamo, R. Cammi, J. W. Ochterski, R. L. Martin, K. Morokuma, O. Farkas, J. B. Foresman, D. J. Fox, Wallingford, Gaussian 16, CT 2016.

3 N. O. C. Winter and C. Hättig, *J. Chem. Phys.*, 2011, **134**, 184101.

4 a. d. o. U. o. K. a. F. TURBOMOLE V7.4 2017 and -. Karlsruhe GmbH, TURBOMOLE GmbH, since S105 2007, 1989-2007.

5 S. Hirata and M. Head-Gordon, *Chem. Phys. Lett.*, 1999, **314**, 291–299.

6 T. H. Dunning Jr., *J. Chem. Phys.*, 1989, **90**, 1007–1023.

7 S. Grimme, *Chem. Phys. Lett.*, 1996, **259**, 128–137.

8 X. Gao, S. Bai, D. Fazzi, T. Niehaus, M. Barbatti and W. Thiel, *J. Chem. Theory Comput.*, 2017, **13**, 515–524.

9 *Nielsen, A.B. and Holder, A.J. (2009) Gauss View 5.0, User's Reference. GAUSSIAN Inc.*

10 N. O. C. Winter and C. Hättig, *J. Chem. Phys.*, 2011, **134**, 184101.

11 Koichi Momma and Fujio Izumi, *J. Appl. Crystallogr.*, 2008, **41**, 653–658.

12 W. Humphrey, A. Dalke and K. Schulten, *J. Mol. Graph.*, 1996, **14**, 33–38.

13 N. M. O'Boyle, A. L. Tenderholt and K. M. Langner, *J Comput Chem*, 2008, **29**, 839–845.

14 J. D. Hunter, *Computing in Science & Engineering*, 2007, **9**, 90–95.

15 M. M. McKerns, L. Strand, T. Sullivan, A. Fang, M. A. G. Aivazis and S. M. J. van der Walt, 2011.

16 O. S. Lee and E. Zysman-Colman, Silico (version 4), DigichemCo, 2023.

17 N. G. Connelly and W. E. Geiger, *Chem. Rev.*, 1996, **96**, 877–910.

18 C. M. Cardona, W. Li, A. E. Kaifer, D. Stockdale and G. C. Bazan, *Adv. Mater.*, 2011, **23**, 2367–2371.

19 G. A. Crosby and J. N. Demas, *J. Phys. Chem.*, 1971, **75**, 991–1024.

20 W. H. Melhuish, *J. Phys. Chem.*, 1961, **65**, 229–235.

21 K. Masui, H. Nakanotani and C. Adachi, *Org. Electron.*, 2013, **14**, 2721–2726.

22 Y. Tsuchiya, S. Diesing, F. Bencheikh, Y. Wada, P. L. dos Santos, H. Kaji, E. Zysman-Colman, I. D. W. Samuel and C. Adachi, *J. Phys. Chem. A*, 2021, **125**, 8074–8089.

23 S. Wu, L. Zhang, J. Wang, A. Kumar Gupta, I. D. W. Samuel and E. Zysman-Colman, *Angew. Chemie Int. Ed.*, 2023, **62**, e202305182.

24 S. Wu, A. Kumar Gupta, K. Yoshida, J. Gong, D. Hall, D. B. Cordes, A. M. Z. Slawin, I. D. W. Samuel and E. Zysman-Colman, *Angew. Chem.Int. Ed.* 2022,**61**, 202213697.

25 S. Wu, W. Li, K. Yoshida, D. Hall, S. Madayanad Suresh, T. Sayner, J. Gong, D. Beljonne, Y. Olivier, I. D. W. Samuel and E. Zysman-Colman, *ACS Appl. Mater. Interfaces*, 2022, **14**, 19, 22341–22352.

26 F. Huang, K. Wang, Y. Z. Shi, X. C. Fan, X. Zhang, J. Yu, C. S. Lee and X. H. Zhang, *ACS Appl. Mater. Interfaces*, 2021, **13**, 36089–36097.

27 D. Sun, S. M. Suresh, D. Hall, M. Zhang, C. Si, D. B. Cordes, A. M. Z. Slawin, Y. Olivier, X. Zhang and E. Zysman-Colman, *Mater. Chem. Front.*, 2020, **4**, 2018–2022.

28 J. F. Liu, S. N. Zou, X. Chen, S. Y. Yang, Y. J. Yu, M. K. Fung, Z. Q. Jiang and L. S. Liao, *Mater Chem Front*, 2022, **6**, 966–972.

29 S. N. Zou, C. C. Peng, S. Y. Yang, Y. K. Qu, Y. J. Yu, X. Chen, Z. Q. Jiang and L. S. Liao, *Org Lett*, 2021, **23**, 958–962.

30 J. Marques dos Santos, C.-Y. Chan, S. Tang, D. Hall, ab Tomas Matulaitis, D. B. Cordes, A. M. Z Slawin, Y. Tsuchiya, L. Edman, C. Adachi, Y. Olivier and E. Zysman-Colman, *J. Mater. Chem. C*, 2023, **11**, 8263.

31 X. C. Fan, K. Wang, Y. Z. Shi, J. X. Chen, F. Huang, H. Wang, Y. N. Hu, Y. Tsuchiya, X. M. Ou, J. Yu, C. Adachi and X. H. Zhang, *Adv Opt Mater*, 2022, **10**, 2101789.